Available online at www.sciencedirect.com

ScienceDirect

ELSEVIER

International Journal of HYDROGEN ENERGY
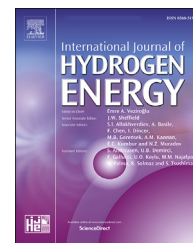
A facile approach to improve the electrochemical properties of polyaniline-carbon nanotube composite electrodes for highly flexible solid-state supercapacitors

Haihan Zhou[*], *Xiaomin Zhi*, *Hua-Jin Zhai*[**]

Institute of Molecular Science, Key Laboratory of Materials for Energy Conversion and Storage of Shanxi Province, Key Laboratory of Chemical Biology and Molecular Engineering of Ministry of Education, Shanxi University, Taiyuan, 030006, China

ARTICLE INFO

ABSTRACT

We seek to improve the electrochemical properties of supercapacitor via engineering the interface of electroactive material/current collector. A facile electrochemical method is put forward to fabricate expanded graphite (ExGP), and polyaniline-carbon nanotube (PANI-CNT) composite electrodes using ExGP as substrate are prepared by one-step co-electro-deposition. Compared with PANI-CNT/GP electrodes, PANI-CNT/ExGP electrodes show significantly improved electrochemical capacitive performances due to reduced constriction/spreading resistance. This effect is ascribed to the increased area of contact points at the interface of electroactive material/current collector for the latter. The PANI-CNT/ExGP electrodes deliver a specific capacitance of 826.7 F g^{-1}, higher than previous reports based on PANI-CNT composites. A highly flexible solid-state supercapacitor is assembled using PANI-CNT/ExGP electrodes. The device shows high rate capability, superior energy/power characteristics (7.1 kW kg^{-1} at an energy density of 12.0 Wh kg^{-1}), and good cycling stability. This study demonstrates that optimizing electroactive material/current collector interface can implement faster electron transport and represents an effective strategy to promote electrochemical capacitive properties of supercapacitors.

Introduction

Supercapacitors have attracted wide interests as one kind of energy storage systems, due to their larger energy density relative to conventional capacitors and higher power density and longer cycle life when compared with batteries. These characteristics enable their applications in consumer electronics, medical devices, and hybrid electric vehicles [1–3]. Depending on electrode materials and operational mechanism, supercapacitors can be classified into two types. One type is electric double-layer capacitors that use carbon materials as electrodes, which store energy via electrostatic charge accumulation at the electrode-electrolyte interface. The other type is pseudocapacitors, commonly utilizing

transition metal oxides and conducting polymers (CPs) to store energy through fast surface redox reaction [4–6].

Of all known CPs, polyaniline (PANI) has been extensively studied owing to its high pseudocapacitance, small mass density, low cost, and environmental friendliness. However, the low electrical conductivity in dedoped state and poor cycle performance, due to swelling and shrinkage during charging/discharging, restrict its practical applications for supercapacitors [7–9]. Carbon nanotubes (CNTs) are another promising material for supercapacitors with high conductivity, large surface area, long cycle life, and high mechanical strength. Nonetheless, CNTs have rather low specific capacitance due to their charge storage mechanism based on electric double-layer [10,11]. Thus, composites based on PANI and CNT have been explored to achieve enhanced electrochemical performance, which combine the advantages of various electrode materials and make use of their synergetic effects [12–16].

In previous reports, PANI-CNT composites based supercapacitor electrodes were prepared by a variety of methods such as chemical oxidative polymerization with soft template [17], chemical vapor deposition and electrodeposition [18], step electrospinning process [19], enzymatic synthesis [20], reverse microemulsion polymerization [21], dispersion filtration [22], and so on. Broadly, these methods can be categorized into two groups, that is, chemical and electrochemical processes. For chemical synthesis, electroactive materials are usually obtained in the form of powder, which requires mixing thoroughly with a polymer binder. Then the resulting paste is pressed onto the current collectors to construct electrodes. The participation of polymeric binder would decrease electrical conductivity of electroactive materials, leading to reduced electrochemical performances. In contrast, electrochemical synthesis is an attractive way to prepare binder-free electrodes, which directly grows electroactive materials on substrates (that is, current collectors), enabling one-pot preparation. In either chemical or electrochemical synthesis, a high-quality interfacial contact between active materials and current collector is desirable in order to reduce contact resistance. However, frequently used current collectors such as stainless steel, carbon cloth, and graphite foil show a flat surface, resulting in a limited number of contact spots between active materials and current collectors [23]. Small contact spot area will inevitably lead to a constriction/spreading resistance at the interface when current flow passes through it [24,25], thereby lowering the electrochemical performances.

Current collector in a supercapacitor serves to collect/transport electrons from/to electroactive materials during charge/discharge [26]. Unfortunately, its role has not received the attention it deserves as compared to electroactive materials. Graphite (GP) is a commercially available paper-like material, which serves routinely as current collectors, featuring low price, high conductivity, and superior mechanical flexibility [27,28]. In this work, we propose a facile electrochemical method to prepare surface expanded graphite (ExGP) in order to offer substantially increased contact points at the active materials/current collector interface. New type of PANI-CNT/ExGP composite electrodes were fabricated via co-electrodeposition of PANI-CNT composite on ExGP substrate.

Correspondingly, the PANI-CNT/ExGP electrodes demonstrated significantly improved electrochemical performances with respect to PANI-CNT/GP electrodes.

Currently the demand for wearable and portable electronic devices has accelerated the development of flexible supercapacitors, which have high flexibility against deformation. Such electronic devices are required to be integrated with a flexible energy storage component as power supply [29–31]. To verify the feasibility for flexible supercapacitor applications, a symmetrical and flexible supercapacitor device was constructed herein using PANI-CNT/ExGP electrodes. This device shows high flexibility and superior supercapacitive performances, thus holding great promise for use in wearable and portable electronics.

Experimental

Chemicals

Aniline (analytical pure) was purchased from Sinopharm. Pristine multi-walled CNTs (outer diameter: < 8 nm) were obtained from Chengdu Organic Chemicals. Poly (sodium 4-styrenesulfonate) (PSS) was supplied by Alfa Aesar. Graphite papers were obtained from Qingdao Herita graphite. All experiments were implemented using deionized (DI) water (18.25 MΩ cm, 24 °C).

Electrode preparation

Graphite papers were cut into a rectangular shape and insulated with adhesive tape to expose conductive areas of 1×1 cm^2 for electrochemical expansion and electrodeposition. Prior to use, they were cleaned in acetone and DI water, successively. Electrochemical expansion of GP was performed using a two-electrode configuration in 1 mM PSS aqueous electrolyte. Here GP (acting as working electrode) was placed in parallel to the Pt foil (as counter electrode). A static potential of 10 V was applied on GP for 40 min to obtain electrochemically expanded GP (ExGP). To increase conductivity, the ExGP was further reduced in a three-electrode configuration in oxygen-free 1 M LiClO$_4$ at −1.2 V vs. saturated calomel electrode (SCE) for 5 min. The obtained ExGP was washed with DI water to remove inorganic residuals.

For carboxylation of CNTs, multi-walled CNTs were pretreated in 3 M HNO$_3$ at 140 °C under magnetic stirring by refluxing for 96 h. Subsequently, they were transferred into a mixture of concentrated H$_2$SO$_4$ and HNO$_3$ (volume ratio 3:1) and functionalized with carboxyl groups under bath-sonication at 40 °C for 2 h. Finally, the resultant carboxylated CNTs (or CNT-COOH) were rinsed with abundant DI water until the pH reaches about 6.0 and dried at 60 °C for 1 day.

PANI-CNT/ExGP electrodes were prepared via electrochemical co-deposition in the aqueous deposition bath consisting of 0.2 M aniline, 0.5 M HCl, and 1 mg mL^{-1} CNT-COOH, which were adequately dispersed by stirring and ultrasonication prior to deposition. Here ExGP was used as the electrodeposition substrate. SCE and Pt sheet were used as reference and counter electrodes, respectively. Electrodeposition was

carried out in the above-mentioned, three-electrode cell with a constant potential of 0.9 V vs. SCE. The total charge passed was set at $1.0\,C\,cm^{-2}$. For comparison, PANI-CNT/GP electrodes were fabricated using the same electrodeposition system and procedure, with GP as substrate. Likewise, PANI/GP electrodes were obtained in the aqueous deposition bath consisting of 0.2 M aniline and 0.5 M HCl with GP as substrate. Loading amount of active materials for PANI/GP, PANI-CNT/GP, and PANI-CNT/ExGP electrodes were measured to be 0.45, 0.40, and 0.40 mg, respectively, with a Mettler-Toledo microbalance (accuracy of 0.01 mg).

Supercapacitor assembly

Flexible symmetric solid-state supercapacitors were fabricated by sandwiching two pieces of identical PANI-CNT/ExGP electrodes with a PVA-H_2SO_4 gel electrolyte, after which the devices were placed in the air at room temperature to vaporize excess water. The gel electrolyte was prepared by mixing 1 g H_2SO_4 and 1 g PVA powder into 10 mL DI water. The mixture was subjected to vigorous stirring at 85 °C until it became clear. The gel electrolyte was obtained after cooling the solution down.

Characterizations

FT-IR spectra were measured with Bruker Tensor 27 FT-IR spectrometer. Morphologies of samples were examined using JEOL JSM-6701F SEM. Raman spectra were obtained at room temperature using a ThermoFisher DXR Raman microscope with a 633 nm laser source. Electrochemical measurements including cyclic voltammetry (CV), galvanostatic charge-discharge (GCD), and electrochemical impedance spectra (EIS) of the electrodes were conducted on a Chenhua CHI 660E electrochemical workstation with symmetric two-electrode configuration using 1 M HCl aqueous electrolyte. EIS were recorded at open circuit potential with a frequency range from 10^5 to 10^{-2} Hz by applying an AC sinusoid signal of 5 mV amplitude.

Results and discussion

Electrochemical expansion of GP

During electrochemical expansion, plenty of mild and small bubbles were generated on GP surface when a bias voltage was applied on it, which originate from O_2 produced by oxidation of water. Meanwhile, defective sites at the edges or grain boundaries of GP opened up due to oxidation. Bubbles within graphitic layers can exert sufficient forces to separate graphite layers, resulting in the expansion of GP. In this study, in order to control the degree of expansion of GP and keep the ExGP standing on the surface of GP substrate, we limited the concentration of PSS electrolyte to 1 mM, which prevented full exfoliation of graphite into solution. When the electrolyte
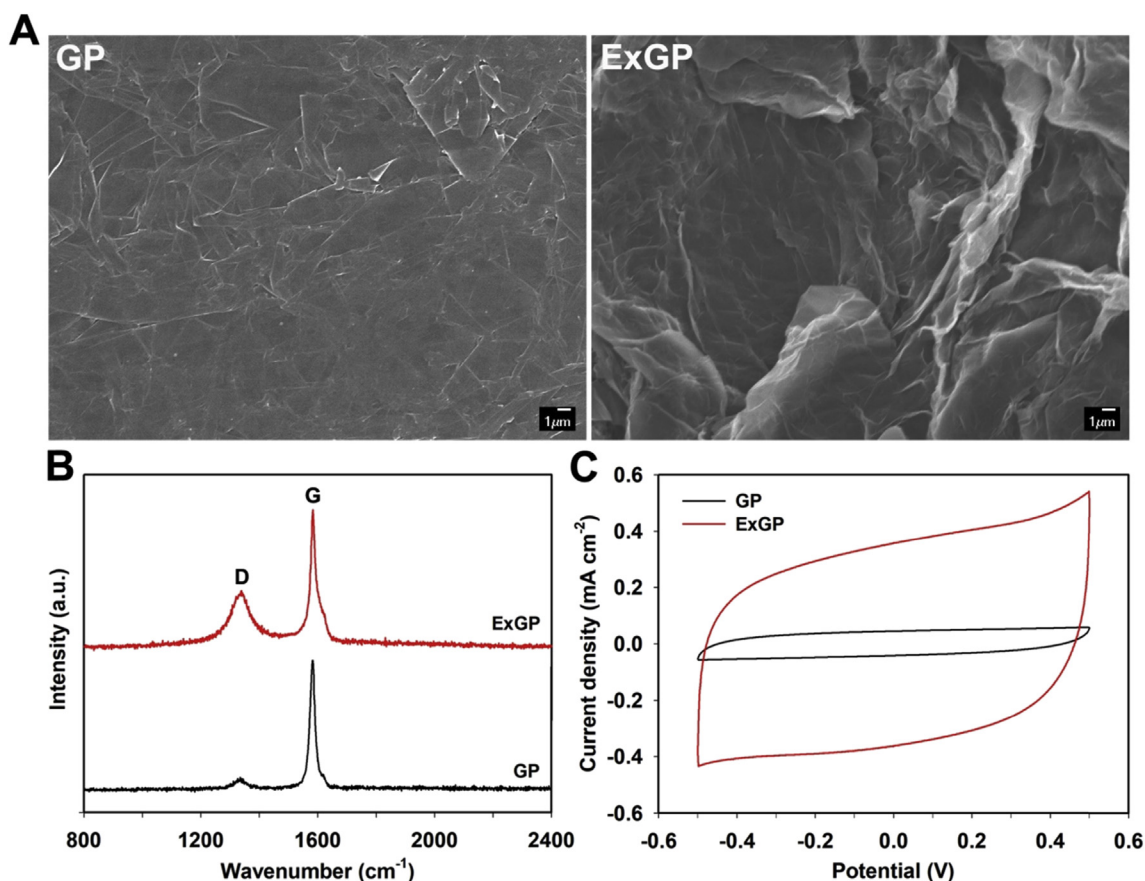
Fig. 1 — (A) SEM images, (B) Raman spectra, and (C) CV curves at 20 mV s^{-1} tested in 1 M KCl for GP and ExGP.

concentration is relatively high (such as 0.01 M), lots of intense and big bubbles were produced due to high current density. In such cases, the GP would be expanded fully and exfoliated into solution to form graphite suspensions.

Fig. 1A shows the SEM images of GP before and after electrochemical expansion. It is clear that GP has a flat morphology, in which graphite sheets tightly stack together. After expansion, GP surface is altered to a curled morphology for ExGP, featuring some wrinkled paper-like structures. Raman spectroscopy is routinely used to characterize ordered and disordered crystal structures of carbon. Fig. 1B compares the Raman spectra of GP and ExGP. Both spectra show graphitic carbon-based characteristic peaks at 1583 cm^{-1} (G band) and 1332 cm^{-1} (D band), corresponding to the first order scattering of the E_{2g} vibration mode of sp^2-hybrid carbon and edges and structure defects on carbon basal planes, respectively [32,33]. Compared to GP, ExGP has an increased intensity ratio of D band to G band (I_D/I_G), which is attributed to partial disorder of graphite crystal after electrochemical expansion. Nonetheless, the low I_D/I_G for ExGP indicates that its structural defects remain at a low level, ensuring a high graphitic structural quality for charge transfer as current collector [34,35]. Electrochemical behavior of GP before and after electrochemical expansion was characterized by CV. As shown in Fig. 1C, ExGP electrode has significantly larger CV area than

GP, which is ascribed to distinctly increased surface area for ion access in the former, in line with its highly open and porous architecture.

Material characterizations

Surface morphologies of PANI and PANI-CNT composite are shown in Fig. 2. PANI exhibits intertwined fiber-shaped microstructures. For PANI-CNT composite, apart from fibrous PANI, it is obvious that amounts of CNTs are closely distributed within PANI fibers. The close contact between CNT and PANI suggests that CNT sort of acts like binder and conductive additive, which shortens the distance of the relatively dispersive PANI fibers and facilitates electrical contact among them. Furthermore, the diameter of these CNTs is approximately 30 nm, much larger than that of as-received CNTs (<8 nm). This observation indicates that a uniform PANI layer is coated on CNT, thus forming CNT@PANI core-shell structure, which results in an increase in diameter. The core-shell structure offers more active sites for pseudocapacitive reaction, due to the promoted dispersion of PANI as coating on the CNTs with large surface area. Additionally, charge carriers on the PANI layer, during pseudocapacitive reaction, can reach highly conductive CNTs via a minimal distance (radial direction). Such a process transports charge carriers efficiently and can achieve high specific capacitance.

Fig. 3 shows FT-IR spectra of CNT, carboxylated CNT, PANI, and PANI-CNT. Compared to CNT, CNT-COOH exhibits an additional peak (1715 cm^{-1}), due to C=O stretching vibration
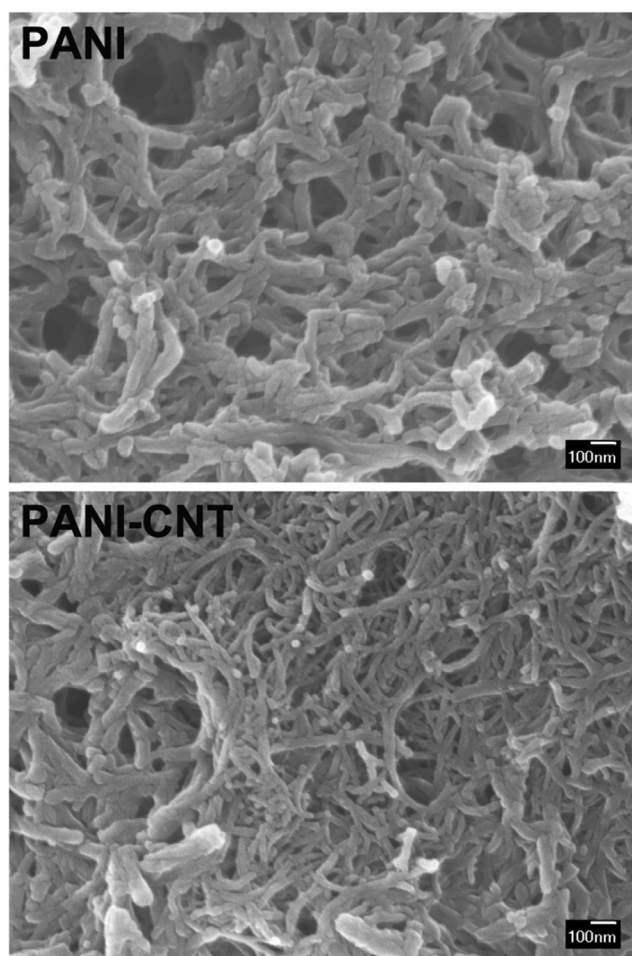
Fig. 2 — SEM images of PANI and PANI-CNT composite.
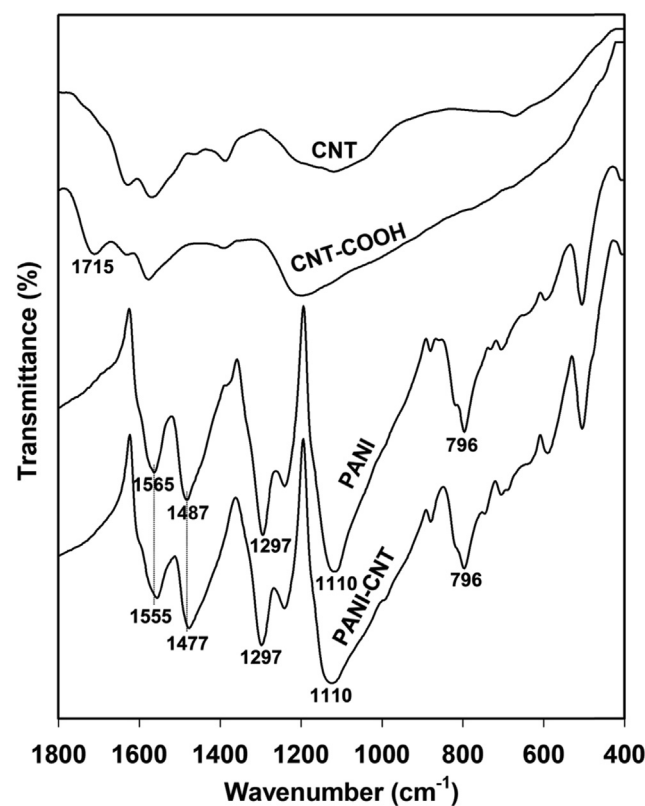
Fig. 3 — FT-IR spectra of CNT, CNT-COOH, PANI, and PANI-CNT.

in carboxyl groups [36], which indicates that carboxyl groups were introduced successfully into CNT through acid treatment. Here negatively charged CNT-COOH acts as dopant/counter anion to neutralize the positively charged, oxidized PANI backbone during electrochemically oxidative polymerization, thereby forming the above-mentioned CNT@PANI core-shell structure. For pure PANI, the characteristic peaks at 1565 and 1487 cm^{-1} are assigned to C=C stretchings of quinoid and benzenoid rings, respectively. The peak at 1297 cm^{-1} belongs to C–N stretching vibration. The absorption at 1110 cm^{-1} corresponds to C=N stretching and the band at 796 cm^{-1} originates from out-of-plane C–H motion [17,21]. As compared to PANI, PANI-CNT composite shows the same peaks, indicating the presence of PANI in the composite. The difference is that typical C=C bonds in PANI at 1565 and 1487 cm^{-1} are red-shifted to 1555 and 1477 cm^{-1} in PANI-CNT, respectively, which is ascribed to the interaction between CNT and π-electrons of PANI chains [37]. In short, the FT-IR data further indicate that PANI-CNT composite was prepared successfully by one-step electrochemical co-deposition.

Electrochemical measurements

CV curves at the scan rate of 10 mV s^{-1} of PANI/GP, PANI-CNT/GP, and PANI-CNT/ExGP electrodes are presented in Fig. 4A. The three types of electrodes show the same pair of redox peaks, which are attributed to redox transition of PANI between leucoemeraldine and polaronic emeraldine forms, as well as the emeraldine—pernigraniline transformation [38]. Compared to PANI/GP, the PANI-CNT/GP electrode has larger area enclosed by the CV curve, indicating that the incorporation of CNT enhances the capability of charge storage. Also it is obvious that PANI-CNT/ExGP electrode has much higher redox peak current, as well as much larger CV area, than PANI/GP and PANI-CNT/GP, suggesting increased specific capacitance. Furthermore, as shown in Fig. 4B, the anodic and cathodic peak current of PANI-CNT/ExGP electrode exhibits nearly a linear increase accompanying increased CV scan rates, implying that the electrode kinetics is surface-controlled redox process [39]. In particular, redox peaks are clearly present up to a high scan rate of 200 mV s^{-1}, revealing that the electrode is beneficial to fast redox reaction. In the meantime, the overall CV shapes nearly do not change, maintaining excellent symmetry in cathodic and anodic directions as scan rate increases. These features suggest that PANI-CNT/ExGP electrode has high-power characteristics and good electrochemical reversibility.

To further compare the electrochemical capacitive behaviors of PANI/GP, PANI-CNT/GP, and PANI-CNT/ExGP electrodes, GCD tests were carried out at a series of current densities ranging from 0.5 to 20 A g^{-1}. Fig. 4C shows the GCD curves of the three types of electrodes at current densities of 2
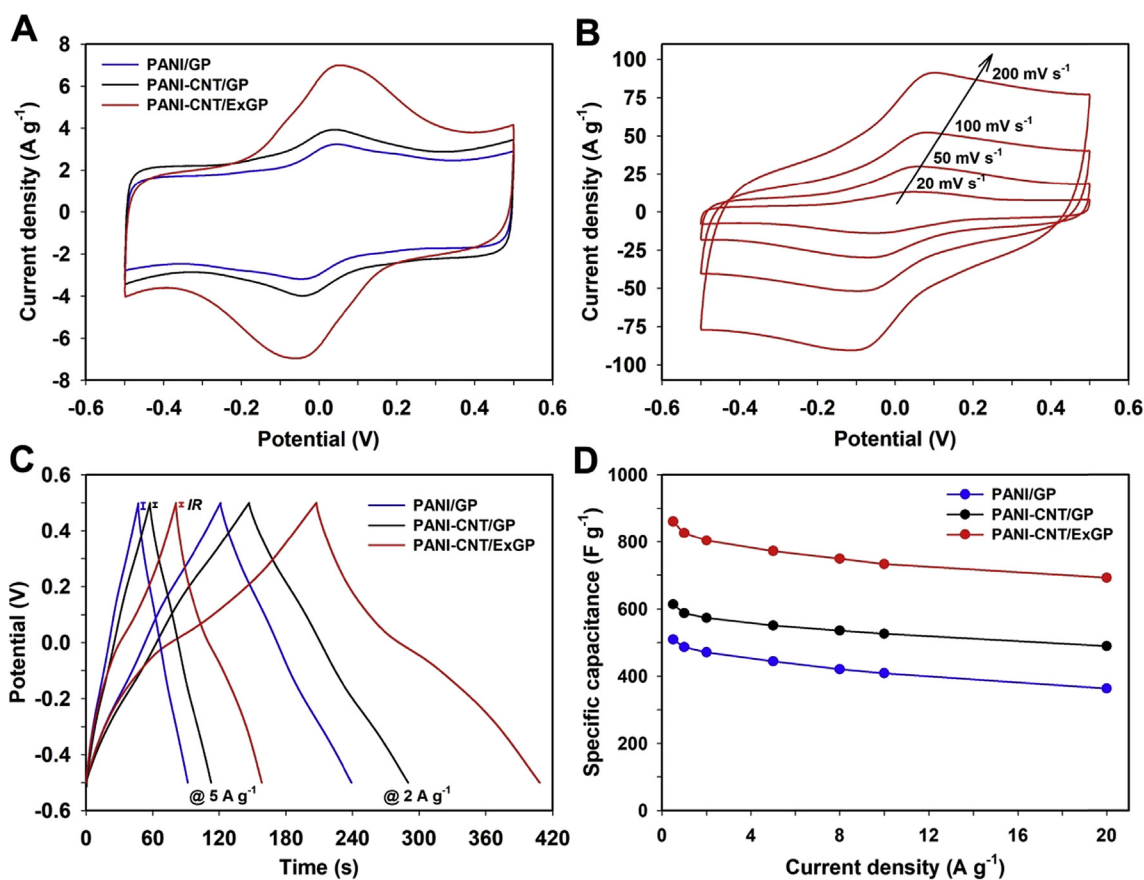
Fig. 4 — (A) CV curves at 10 mV s^{-1} for PANI/GP, PANI-CNT/GP, and PANI-CNT/ExGP electrodes. (B) CV curves of PANI-CNT/ExGP electrode at the scan rates ranging from 20 to 200 mV s^{-1} (C) GCD curves at 2 and 5 A g^{-1} and (D) plots of specific capacitance *vs.* GCD current densities for PANI/GP, PANI-CNT/GP, and PANI-CNT/ExGP electrodes.

and 5 A g^{-1}. Three observations are evident from the GCD curves. First, PANI-CNT/ExGP electrode has the longest discharge time and hence the highest specific capacitance. Second and more importantly, PANI-CNT/ExGP electrode also shows obvious deviation from linearity in GCD curves in comparison with PANI/GP and PANI-CNT/GP, indicating that PANI-CNT/ExGP has significantly improved pseudocapacitive character during charging-discharging, in line with CV results. Third, PANI-CNT/ExGP electrode exhibits the lowest IR drop caused by internal resistance, which is crucial for supercapacitors, because it will decrease the production of unwanted heat during the charge-discharge process [40,41].

Specific capacitance (C in F g^{-1}) of electrodes can be calculated by the following equation: C = $(2 \times I \times t)/(\Delta V \times m)$, where I is the discharge current in A, t the discharge time in s, ΔV the potential window tested in V, and m the loading amount of active material in g. Fig. 4D shows that PANI-CNT/ExGP electrode achieve significantly increased specific capacitance at various current densities as compared to PANI-CNT/GP, with PANI/GP delivering the lowest specific capacitance. At current density of 1 A g^{-1}, the specific capacitance of PANI/GP and PANI-CNT/GP electrodes is 486.4 and 587.1 F g^{-1}, respectively, whereas that of PANI-CNT/ExGP electrode rises to as high as 826.7 F g^{-1} (that is, a boost of at least 40%). The latter value is also higher than other PANI-CNT composites based electrodes in previous reports (see Table 1). In addition, PANI-CNT/ExGP electrode still maintains a high specific capacitance of 692.6 F g^{-1} as GCD current density is increased to 20 A g^{-1}, demonstrating superior rate capability. Compared with PANI/GP electrode, the enhanced capacitive performances of PANI-CNT/GP electrode can be ascribed to the

introduction of highly conductive CNTs, which facilitates the contact and charge transfer of PANI fibers. Its advantages also originate from the CNT@PANI core-shell structure, as described in the SEM characterization. In contrast to PANI-CNT/GP, the significantly improved electrochemical capacitive properties for PANI-CNT/ExGP electrode can be explained as follows.

As schematically shown in Fig. 5 (top), there are only very limited contact points at the interface of PANI-CNT films and current collector, due to smooth surface topography for GP. This implies that electrons within active materials, especially those far from contact points, have to run a long distance to reach the current collector. Subsequently, these electrons go through and spread out of the constriction in order to complete the charge transport processes. However, a considerable constriction/spreading resistance will be inevitably generated at the interface due to the restriction of current flow by small contact spot area [24,25], which affects the electrochemical performances of PANI-CNT/GP electrode. Unlike such a detoured electron transport for GP, ExGP can provide a substantially increased number of contact points due to plenty of curly graphite sheets on its surface, thus significantly reducing the constriction/spreading resistance, as illustrated in Fig. 5 (bottom). Here electrons are anticipated to be transported through the nearest contact point to the current collector. The curly graphite sheets act like "bridges" to offer high-quality electrical links at the interface of active materials and current collector, which provide more pathways for electron transport, markedly shortening the distance between electrons and current collector. In addition, we think that both chemisorption and physisorption occur between PANI-CNT

Preparation approaches	Performance			References
	Electrolyte	Scan rate/Current density	Specific capacitance	
Chemical polymerization	1 M H$_2$SO$_4$	2 mV s^{-1}	540.3 F g^{-1}	[12]
Ultrasonic polymerization	1 M NaNO$_3$	0.5 A g^{-1}	201 F g^{-1}	[13]
In situ chemical oxidative polymerization	1 M H$_2$SO$_4$	10 mV s^{-1}	294 F g^{-1}	[14]
In situ electropolymerization	1 M KOH	1.6 A g^{-1}	296 F g^{-1}	[15]
Filtration and electrical synergy	6 M KOH	0.5 A g^{-1}	146.0 F g^{-1}	[16]
Chemical oxidative polymerization with soft template	0.5 M H$_2$SO$_4$	0.5 A g^{-1}	348.9 F g^{-1}	[17]
Chemical vapor deposition and electrodeposition	1 M H$_2$SO$_4$	1.56 mA cm^{-2}	359 F g^{-1}	[18]
Step electrospinning process	1 M H$_2$SO$_4$	0.5 A g^{-1}	385 F g^{-1}	[19]
Enzymatic synthesis	1 M H$_2$SO$_4$	5 mV s^{-1}	440 F g^{-1}	[20]
Reverse microemulsion polymerization	1 M H$_2$SO$_4$	0.5 A g^{-1}	663 F g^{-1}	[21]
Dispersion filtration	3 M H$_2$SO$_4$	10 mV s^{-1}	448 F g^{-1}	[22]
Nanocasting technique using plant leave template	1 M H$_2$SO$_4$	1 A g^{-1}	535 F g^{-1}	[37]
Chemical oxidative polymerization	0.5 M H$_2$SO$_4$	0.5 A g^{-1}	368.4 F g^{-1}	[42]
In situ chemical polymerization	1 M H$_2$SO$_4$	1 A g^{-1}	315 F g^{-1}	[43]
Chemical oxidative process	1 M H$_2$SO$_4$	1 A g^{-1}	381 F g^{-1}	[44]
In situ potentiostatic deposition	1 M H$_2$SO$_4$	10 mA cm^{-2}	463 F g^{-1}	[45]
In situ polymerization	0.1 M H$_2$SO$_4$	1 mV s^{-1}	560 F g^{-1}	[46]
In situ oxidative polymerization	1 M H$_2$SO$_4$	20 mV s^{-1}	515.2 F g^{-1}	[47]
In situ electrochemical polymerization	0.5 M H$_2$SO$_4$	5 mA cm^{-2}	500 F g^{-1}	[48]
Electrospinning and in situ polymerization	1 M H$_2$SO$_4$	0.3 A g^{-1}	503 F g^{-1}	[49]
Chemical vapor deposition and electrodeposition	1 M H$_2$SO$_4$	5 mV s^{-1}	746 F g^{-1}	[50]
In situ chemical oxidative polymerization	1 M HCl	30 mV s^{-1}	762 F g^{-1}	[51]
Flow-directed assembly and reoxidation and redoping	1 M HCl	0.1 A g^{-1}	569 F g^{-1}	[52]
Electrochemical expansion and codeposition	1 M HCl	1 A g^{-1}	826.7 F g^{-1}	This work

Table 1 — Specific capacitance for PANI-CNT composite based electrodes obtained in this work, as compare to those reported previously using different approaches.
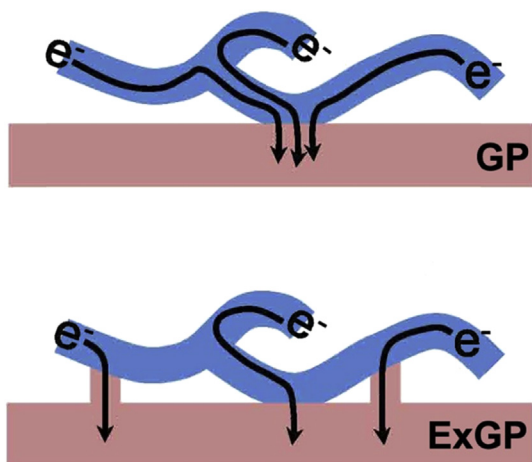
Fig. 5 — Schematic of the electron transport processes between PANI-CNT films and different current collectors, including GP (top) and ExGP (bottom).

films and ExGP [53—57]. Apart from physisorption based on van der Waals force, chemisorption exists because oxygen-containing functional group on ExGP can act as doping anions during electropolymerization of PANI-CNT films.

Supercapacitor tests

To explore potential application in flexible supercapacitors, a solid-state supercapacitor device was assembled by two pieces of symmetric PANI-CNT/ExGP electrodes with PVA-H_2SO_4 gel electrolyte sandwiched in between. Fig. 6A shows that the device maintains nearly unchanged CV profile and substantially increased current response as CV scan rate increases. Besides, redox peaks still can be observed up to 100 mV s^{-1}, indicating fast charge transfer kinetics. The GCD curves in Fig. 6B show good symmetry and almost linear slopes at current densities ranging from 2 to 20 A g^{-1}, suggesting high coulombic efficiency and fast Faraday redox reaction [58]. Fig. 6C presents the rate capability of the device, which retains 70.2% of its capacitance as GCD current density increases 20 times from 1 to 20 A g^{-1}. Additionally, the as-prepared device has rather high mechanical flexibility, so that it can even endure bend up to 180° without destroying its construction; see the inset of Fig. 6C.

EIS was measured to further understand electrochemical behaviors of the supercapacitor. Fig. 7A shows the Nyquist plot, which has a vertical trend at low-frequency region, demonstrating ideal capacitive behavior. The inset of Fig. 7A gives a well-fitted equivalent circuit. Here R_e is the equivalent series resistance, which is an important factor that affects the power density. Equivalent series resistance is a combination of ionic resistance of electrolyte, intrinsic resistance of active material, and contact resistance at the active material/current collector interface. Furthermore, R_{ct} represents charge transfer resistance at the electrode/electrolyte interface, W the Warburg resistance related to ion diffusion/transport from electrolyte to electrode surface, and CPE the constant phase element. The R_e, R_{ct}, and W values are 4.8, 1.1, and 4.6 Ω, respectively. These small values affirm the fast charge
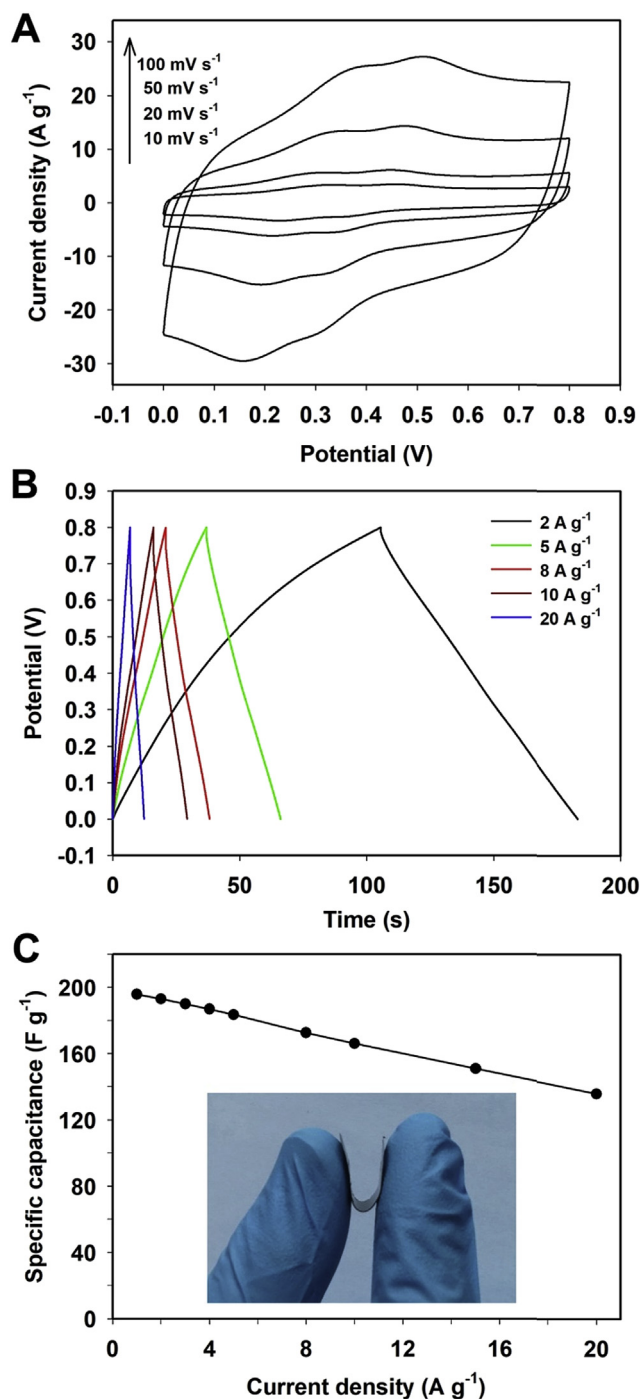
Fig. 6 — (A) CV profiles at the scan rates ranging from 10 to 100 mV s^{-1}, (B) GCD curves at the current densities from 2 to 20 A g^{-1}, and (C) plot of specific capacitance *vs.* GCD current density for the symmetric PANI-CNT/ExGP based supercapacitor. The inset in (C) is an image showing mechanical deformation of PANI-CNT/ExGP based supercapacitor.

transfer and ion diffusion properties, which are responsible for good capacitive behaviors of PANI-CNT/ExGP based supercapacitor, as supported by the CV and GCD tests.

Specific energy density (E in Wh kg^{-1}) and power density (P in W kg^{-1}) for the tested supercapacitor are calculated
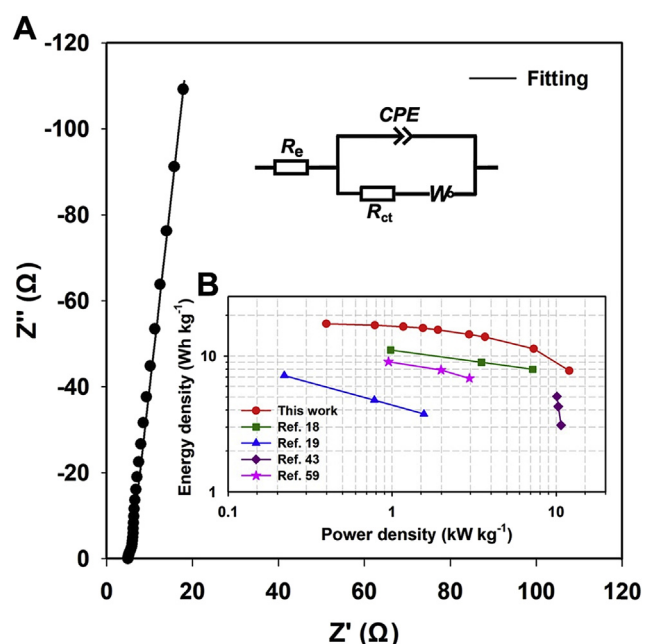
Fig. 7 – (A) EIS Nyquist plot and the fitting curve based on the proposed equivalent circuit (inset). (B) Ragone plot for PANI-CNT/ExGP based supercapacitor, compared to prior reports.

based on the GCD curves using the following equations: $E = 1/2 \times C\Delta V^2$ and $P = E/t$, where ΔV is the potential window (V), C the areal capacitance of supercapacitor (F g^{-1}), and t the discharge time (s). Fig. 7B is the Ragone plot, which shows energy density as a function of power density for PANI-CNT/ExGP based supercapacitor. The highest energy and power
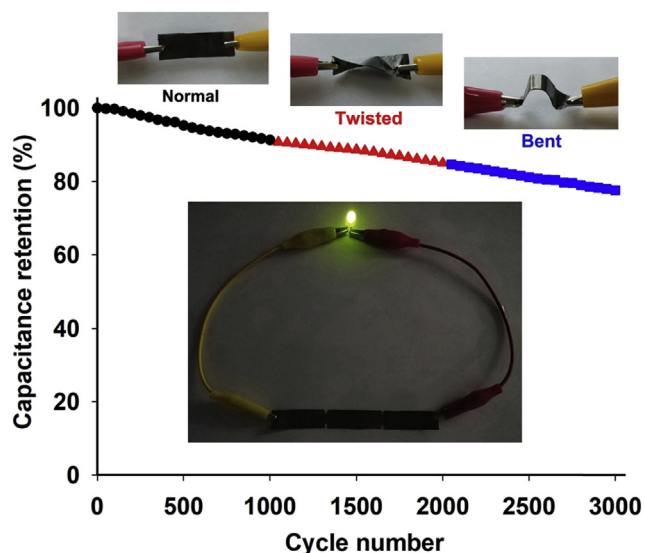
Fig. 8 – Cycle performance tested by CV at 50 mV s^{-1} under normal, twisted, and bent states for the supercapacitor device. The inset shows that three such devices connected in series light up a green LED. (For interpretation of the references to color/colour in this figure legend, the reader is referred to the Web version of this article.)

densities for the device are 17.3 Wh kg^{-1} (at a power density of 0.39 kW kg^{-1}) and 7.1 kW kg^{-1} (at an energy density of 12.0 Wh kg^{-1}), respectively. These values are higher than those reported for supercapacitors based on PANI incorporated with CNT [18,19,43,59]; see comparison in Fig. 7B.

Adaptability of this device for flexible energy storage was verified by cycling test under normal, twisted, and bent states (Fig. 8). Cycle performance was evaluated by CV tests at scan rate of 50 mV s^{-1}. Under normal state, the device maintains 91.3% of the initial capacitance for 1000 cycles, which is better than those reported for composites based on PANI and CNT (78.6–83% for 1000 or 500 cycles) [16,17,19,21]. Next, cycle performance of the device was measured under harsh mechanical deformation conditions, including twisted and bent states. After 3000 cycles, the device retains 78.6% of its initial specific capacitance. In addition to superior electrochemical properties, the good cycle performance is also related to the intimate interfacial contact between components and its high mechanical robustness. Ultimately, the practical applicability of PANI-CNT/ExGP based supercapacitor is demonstrated by using three devices connected in series to power a green LED (2.0 V rated); see the inset of Fig. 8.

Conclusions

We have proposed and implemented a facile method to enhance the electron transport between active material and current collector in supercapacitors, wherein PANI-CNT composite is co-electrodeposited on electrochemically expanded GP (ExGP) as current collector. In comparison to PANI-CNT/GP, the PANI-CNT/ExGP electrode demonstrates significantly improved electrochemical performances. ExGP can provide abundant contact points at the active material/current collector interface, thereby markedly reducing constriction/spreading resistance. The resulting PANI-CNT/ExGP electrode has a high specific capacitance of 826.7 F g^{-1}. The as-fabricated flexible solid-state supercapacitor based on PANI-CNT/ExGP electrodes shows high flexibility and superior electrochemical performances, such as high rate capability, superior energy/power character (7.1 kW kg^{-1} at an energy density of 12.0 Wh kg^{-1}), and good cycling stability (77.6% capacitance retention after 3000 cycles). The device is very promising for high-efficiency flexible energy storage. The present work shall stimulate further research activities on current collectors, a crucial component in supercapacitors. Such studies may help optimize charge transport in supercapacitors and further boost their electrochemical performances.

Acknowledgments

REFERENCES

[1] Zuo WH, Xie CY, Xu P, Li YY, Liu JP. A novel phase-transformation activation process toward Ni-Mn-O nanoprism arrays for 2.4 V ultrahigh-voltage aqueous supercapacitors. Adv Mater 2017;29:1703463.

[2] Wang MQ, Li ZQ, Wang CX, Zhao RZ, Li CX, Guo DX, et al. Novel core-shell FeOF/Ni(OH)$_2$ hierarchical nanostructure for all-solid-state flexible supercapacitors with enhanced performance. Adv Funct Mater 2017;27:1701014.

[3] Wang X, Yang C, Jin J, Li X, Cheng Q, Wang G. High-performance stretchable supercapacitors based on intrinsically stretchable acrylate rubber/MWCNTs@conductive polymer composite electrodes. J Mater Chem A 2018;6:4432–42.

[4] Tian JY, Zhang HY, Liu ZM, Qin G, Li ZH. One-step synthesis of 3D sulfur-doped porous carbon with multilevel pore structure for high-rate supercapacitors. Int J Hydrogen Energy 2018;43:1596–605.

[5] Wang JG, Zhang ZY, Liu XR, Wei BQ. Facile synthesis of cobalt hexacyanoferrate/graphene nanocomposites for high-performance supercapacitor. Electrochim Acta 2017;235:114–21.

[6] Li M, Yuan PW, Guo SH, Liu F, Cheng JP. Design and synthesis of Ni-Co and Ni-Mn layered double hydroxides hollow microspheres for supercapacitor. Int J Hydrogen Energy 2017;42:28797–806.

[7] Sowmya M Selvakumar. Multilayered electrode materials based on polyaniline/activated carbon composites for supercapacitor applications. Int J Hydrogen Energy 2018;43:4067–80.

[8] Zhang QE, Zhou AA, Wang JJ, Wu JF, Bai H. Degradation-induced capacitance: a new insight into the superior capacitive performance of polyaniline/graphene composites. Energy Environ Sci 2017;10:2372–82.

[9] Shao L, Wang Q, Ma Z, Ji Z, Wang X, Song D, et al. A high-capacitance flexible solid-state supercapacitor based on polyaniline and metal-organic framework (UiO-66) composites. J Power Sources 2018;379:350–61.

[10] Chinnappan A, Sandal H, Kim H, Ramakrishna S. Mn nanoparticles decorated on the ionic liquid functionalized multiwalled carbon nanotubes as a supercapacitor electrode material. Chem Eng J 2017;316:928–35.

[11] Sun JK, Zan P, Ye L, Yang XJ, Zhao LJ. Superior performance of ZnCo$_2$O$_4$/ZnO@multiwall carbon nanotubes with laminated shape assembled as highly practical all-solid-state asymmetric supercapacitors. J Mater Chem A 2017;5:9815–23.

[12] Roy A, Ray A, Saha S, Das S. Investigation on energy storage and conversion properties of multifunctional PANI-MWCNT composite. Int J Hydrogen Energy 2018;43:7128–39.

[13] Lee SY, Kim JI, Park SJ. Activated carbon nanotubes/polyaniline composites as supercapacitor electrodes. Energy 2014;78:298–303.

[14] Liu D, Wang X, Deng JX, Zhou CL, Guo JS, Liu P. Crosslinked carbon nanotubes/polyaniline composites as a pseudocapacitive material with high cycling stability. Nanomaterials 2015;5:1034–47.

[15] Wang RR, Wu Q, Zhang XH, Yang ZH, Gao LJ, Ni JF, et al. Flexible supercapacitors based on a polyaniline nanowire-infilled 10 nm-diameter carbon nanotube porous membrane by in situ electrochemical polymerization. J Mater Chem A 2016;4:12602–8.

[16] Zhang JR, Li XY, Wang X, Qiu BW, Li ZJ, Ding J. Preparation of vertically aligned carbon nanotube/polyaniline composite membranes and the flash welding effect on their supercapacitor properties. RSC Adv 2016;6:98598–605.

[17] Arulmani S, Wu JJ, Anandan S. Amphiphilic Triblock Copolymer guided Polyaniline embraced CNT nanohybrid with outcropping whiskers as an energy storage electrode. Electrochim Acta 2017;246:737–47.

[18] Malik R, Zhang L, McConnell C, Schott M, Hsieh YY, Noga R, et al. Three-dimensional, free-standing polyaniline/carbon nanotube composite-based electrode for high-performance supercapacitors. Carbon 2017;116:579–90.

[19] Simotwo SK, DelRe C, Kalra V. Supercapacitor electrodes based on high-purity electrospun polyaniline and polyaniline-carbon nanotube nanofibers. ACS Appl Mater Interfaces 2016;8:21261–9.

[20] Otrokhov G, Pankratov D, Shumakovich G, Khlupova M, Zeifman Y, Vasil'eva I, et al. Enzymatic synthesis of polyaniline/multi-walled carbon nanotube composite with core shell structure and its electrochemical characterization for supercapacitor application. Electrochim Acta 2014;123:151–7.

[21] Guo FJ, Mi HY, Zhou JP, Zhao ZB, Qiu JS. Hybrid pseudocapacitor materials from polyaniline@multi-walled carbon nanotube with ultrafine nanofiber-assembled network shell. Carbon 2015;95:323–9.

[22] Arcila-Velez MR, Emmett RK, Karakaya M, Podila R, Diaz-Orellana KP, Rao AM, et al. A facile and scalable approach to fabricating free-standing polymer-carbon nanotube composite electrodes. Synth Met 2016;215:35–40.

[23] Taberna PL, Mitra S, Poizot P, Simon P, Tarascon JM. High rate capabilities Fe$_3$O$_4$-based Cu nano-architectured electrodes for lithium-ion battery applications. Nat Mater 2006;5:567–73.

[24] Li L, Morris JE. Electrical conduction models for isotropically conductive adhesive joints. IEEE Trans Compon Packag Manuf A 1997;20:3–8.

[25] Abram EJ, Sinclair DC, West AR. Electrode-contact spreading resistance phenomena in doped-lanthanum gallate ceramics. J Electroceram 2001;7:179–88.

[26] Wu ZS, Liu ZY, Parvez K, Feng XL, Müllen K. Ultrathin printable graphene supercapacitors with AC line-filtering performance. Adv Mater 2015;27:3669–75.

[27] Liu YC, Miao XF, Fang JH, Zhang XX, Chen SJ, Li W, et al. Layered-MnO$_2$ nanosheet grown on nitrogen-doped graphene template as a composite cathode for flexible solid-state asymmetric supercapacitor. ACS Appl Mater Interfaces 2016;8:5251–60.

[28] Ramadoss A, Yoon KY, Kwak MJ, Kim SI, Ryu ST, Jang JH. Fully flexible, lightweight, high performance all-solid-state supercapacitor based on 3-Dimensional-graphene/graphite-paper. J Power Sources 2017;337:159–65.

[29] Shinde PA, Lokhande VC, Patil AM, Ji T, Lokhande CD. Single-step hydrothermal synthesis of WO$_3$-MnO$_2$ composite as an active material for all-solid-state flexible asymmetric supercapacitor. Int J Hydrogen Energy 2018;43:2869–80.

[30] Xu C, Li ZH, Yang C, Zou PC, Xie BH, Lin ZY, et al. An ultralong, highly oriented nickel-nanowire-array electrode scaffold for high-performance compressible pseudocapacitors. Adv Mater 2016;28:4105–10.

[31] Balaji SS, Karnan M, Sathish M. Supercritical fluid processing of N-doped graphene and its application in high energy symmetric supercapacitor. Int J Hydrogen Energy 2018;43:4044–57.

[32] Parvez K, Li RJ, Puniredd SR, Hernandez Y, Hinkel F, Wang SH, et al. Electrochemically exfoliated graphene as solution-processable, highly conductive electrodes for organic electronics. ACS Nano 2013;7:3598–606.

[33] Duraia ESM, Fahami A, Beall GW. Modifications of graphite and multiwall carbon nanotubes in the presence of urea. J Electron Mater 2018;47:1176–82.

[34] Belekoukia M, Ramasamy MS, Yang S, Feng XL, Paterakis G, Dracopoulos V, et al. Electrochemically exfoliated graphene/ PEDOT composite films as efficient Pt-free counter electrode for dye-sensitized solar cells. Electrochim Acta 2016;194:110–5.

[35] Liu JZ, Notarianni M, Will G, Tiong VT, Wang HX, Motta N. Electrochemically exfoliated graphene for electrode films: effect of graphene flake thickness on the sheet resistance and capacitive properties. Langmuir 2013;29:13307–14.

[36] Zhou WW, Sasaki S, Kawasaki A. Effective control of nanodefects in multiwalled carbon nanotubes by acid treatment. Carbon 2014;78:121–9.

[37] Chang CM, Weng CJ, Chien CM, Chuang TL, Lee TY, Yeh JM, et al. Polyaniline/carbon nanotube nanocomposite electrodes with biomimetic hierarchical structure for supercapacitors. J Mater Chem A 2013;1:14719–28.

[38] Liang JS, Su SJ, Fang X, Wang DZ, Xu SC. Electrospun fibrous electrodes with tunable microstructure made of polyaniline/ multi-walled carbon nanotube suspension for all-solid-state supercapacitors. Mater Sci Eng B 2016;211:61–6.

[39] Zhang YF, Ma MZ, Yang J, Su HQ, Huang W, Dong XC. Selective synthesis of hierarchical mesoporous spinel $NiCo_2O_4$ for high-performance supercapacitors. Nanoscale 2014;6:4303–8.

[40] Zhang Z, Ren L, Han WJ, Meng LJ, Wei XL, Qi X, et al. One-pot electrodeposition synthesis of ZnO/graphene composite and its use as binder-free electrode for supercapacitor. Ceram Int 2015;41:4374–80.

[41] Wang KL, Cao YH, Gu ZR, Ahrenkiel P, Lee J, Fan QH. Nitrogen-modified biomass-derived cheese-like porous carbon for electric double layer capacitors. RSC Adv 2016;6:26738–44.

[42] Ramana GV, Srikanth VVSS, Padya B, Jain PK. Carbon nanotube-polyaniline nanotube core-shell structures for electrochemical applications. Eur Polym J 2014;57:137–42.

[43] Miao FJ, Shao CL, Li XH, Wang KX, Lu N, Liu YC. Electrospun carbon nanofibers/carbon nanotubes/polyaniline ternary composites with enhanced electrochemical performance for flexible solid-state supercapacitors. ACS Sustain Chem Eng 2016;4:1689–96.

[44] He XP, Liu GL, Yan B, Suo H, Zhao C. Significant enhancement of electrochemical behaviour by incorporation of carboxyl group functionalized carbon nanotubes into polyaniline based supercapacitor. Eur Polym J 2016;83:53–9.

[45] Gupta V, Miura N. Influence of the microstructure on the supercapacitive behavior of polyaniline/single-wall carbon nanotube composites. J Power Sources 2006;157:616–20.

[46] Zhou Y, Qin ZY, Li L, Zhang Y, Wei YL, Wang LF, et al. Polyaniline/multi-walled carbon nanotube composites with core-shell structures as supercapacitor electrode materials. Electrochim Acta 2010;55:3904–8.

[47] Zhu ZZ, Wang GC, Sun MQ, Li XW, Li CZ. Fabrication and electrochemical characterization of polyaniline nanorods modified with sulfonated carbon nanotubes for supercapacitor applications. Electrochim Acta 2011;56:1366–72.

[48] Zhang J, Kong LB, Wang B, Luo YC, Kang L. In-situ electrochemical polymerization of multi-walled carbon nanotube/polyaniline composite films for electrochemical supercapacitors. Synth Met 2009;159:260–6.

[49] Zhou ZP, Wu XF, Hou HQ. Electrospun carbon nanofibers surface-grown with carbon nanotubes and polyaniline for use as high-performance electrode materials of supercapacitors. RSC Adv 2014;4:23622–9.

[50] Zhao WQ, Wang SS, Wang CH, Wu ST, Xu WJ, Zou MC, et al. Double polymer sheathed carbon nanotube supercapacitors show enhanced cycling stability. Nanoscale 2016;8:626–33.

[51] Fathi M, Saghafi M, Mahboubi F, Mohajerzadeh S. Synthesis and electrochemical investigation of polyaniline/unzipped carbon nanotube composites as electrode material in supercapacitors. Synth Met 2014;198:345–56.

[52] Lu XJ, Dou H, Yang SD, Hao L, Zhang LJ, Shen LF, et al. Fabrication and electrochemical capacitance of hierarchical graphene/polyaniline/carbon nanotube ternary composite film. Electrochim Acta 2011;56:9224–32.

[53] Zhao Y, Clar JG, Li LP, Xu J, Yuan TY, Bonzongo JJ, et al. Selective desorption of high-purity (6,5) SWCNTs from hydrogels through surfactant modulation. Chem Commun 2016;52:2928–31.

[54] Clar JG, Yuan TY, Zhao Y, Bonzongo JJ, Ziegler KJ. Evaluation of critical parameters in the separation of single-wall carbon nanotubes through selective adsorption onto hydrogels. J Phys Chem C 2014;118:15495–505.

[55] Xu J, Mueller R, Hazelbaker E, Zhao Y, Bonzongo JJ, Clar JG, et al. Strongly bound sodium dodecyl sulfate surrounding single-wall carbon nanotubes. Langmuir 2017;33:5006–14.

[56] Bian JC, Li Z, Chen ZD, He HY, Zhang XW, Li X, et al. Electrodeposition of silver nanoparticle arrays on ITO coated glass and their application as reproducible surface-enhanced Raman scattering substrate. Appl Surf Sci 2011;258:1831–5.

[57] Labaye DE, Jérôme C, Geskin VM, Louette P, Lazzaroni R, Martinot L, et al. Full electrochemical synthesis of conducting polymer films chemically grafted to conducting surfaces. Langmuir 2002;18:5222–30.

[58] Lu XH, Zhai T, Zhang XH, Shen YQ, Yuan LY, Hu B, et al. WO_{3-x} @Au@MnO_2 core-shell nanowires on carbon fabric for high-performance flexible supercapacitors. Adv Mater 2012;24:938–44.

[59] Meng CZ, Liu CH, Chen LZ, Hu CH, Fan SS. Highly flexible and all-solid-state paperlike polymer supercapacitors. Nano Lett 2010;10:4025–31.